

Chapter 3

Three Dimensional Finite Difference Modeling

As has been shown in previous chapters, the thermal impedance of microbolometers is an important property affecting device performance. In chapter 2, a simple analytical model was utilized by simplifying the device geometry. For more accurate impedance values, or for more complex device structures such as composite microbolometer design, another method must be used. A two dimensional finite element method has been demonstrated for this purpose [1]. For this study, a three dimensional finite difference technique was used to more precisely model the effects of materials and device structures on microbolometer performance.

Even with faster computers, several modifications to the basic algorithm were needed to make three dimensional analysis of these devices feasible with reasonable computer power. This was mainly due to the large number of nodes needed for three dimensional analysis. The wide range of dimensions required that the spacing between nodes be flexible. For example, in the Y-direction, device dimensions (film thickness) may be as little as 500 Å (a minimum of 20 nodes/micron), while the thermally significant region in the vicinity of the device may extend more than 5 μm in three dimensions. If a node spacing of 500 Å is used in all three dimensions for a 5 μm x 5 μm x 5 μm region, a total of 10^6 nodes would be required. This would require excessive memory and would greatly increase computation time. Also, since the more complex device shapes of composite microbolometers have varying cross sections, it would be impractical to require that all device boundaries lie directly on the node sites if the nodes are arranged in a regular rectangular grid pattern. In order to accommodate complex device shapes, the computer program written and discussed for this study allowed device boundaries to fall arbitrarily on or between node centers.

3.1 Steady State Analysis

In order to understand the basis of the formulas and algorithms used for this study, an explanation will be given starting from commonly known principles of heat conduction. One fundamental relation of heat flow is known as *Fourier's Law of Heat Conduction* which states that conductive heat is proportional to a temperature gradient. The one dimensional quantitative form of this relation is given in equation 3.1a:

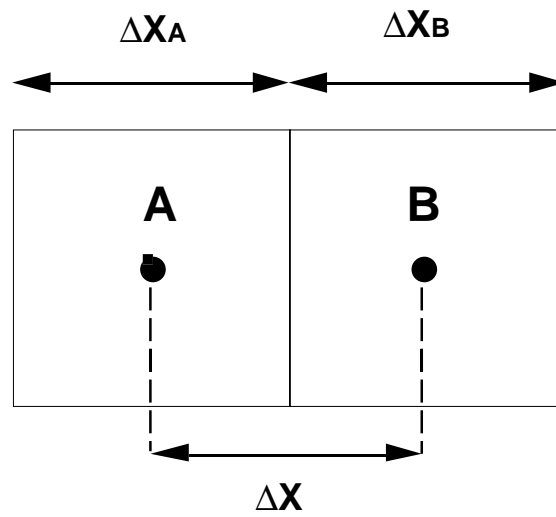
$$q_x = -k \cdot A \cdot \frac{\partial T}{\partial x} \quad [\text{Watts}] \quad (3.1a)$$

where q_x is the heat flux (units of watts/cm²) in the x -direction, k is the thermal conductivity of the material with units of watts/K/cm², A is the cross sectional area, and dT/dx is the thermal gradient in the x -direction. A more general form of this relation is given as:

$$q^{\text{net}} = -k \cdot A \cdot \nabla T \quad [\text{Watts}] \quad (3.1b)$$

where q^{net} is the net heat flux passing through a small region of space.

For complex device shapes, a practical way to model thermal properties is to divide the region into a grid of discrete regular shapes which can be easily modeled individually. Instead of calculating the thermal profile as a continuous function throughout the device, calculations are based on differences in temperature between **nodes** that are spaced a finite distance apart throughout the device. Figure 3.1. illustrates how two adjacent nodes can be used to represent regions being modeled.



a) Two Adjacent Node Volumes

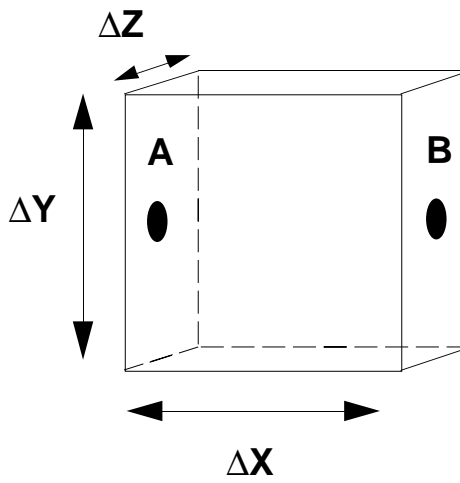
b) Transport Region used to calculate the thermal impedance between nodes **A** and **B**.

Figure 3.1 "Adjacent Nodes"

The **node volume**, illustrated in figure 3.1a, refers to the volume contained within the boundaries of the node. A characteristic temperature of the node is defined as the temperature at a specified point in each node. For these studies, this point is referred to as the **node center**, although this point can be defined anywhere within the node volume. The node **transport region** refers to the volume between two adjacent node centers, as shown in Figure 3.1b. The length of the transport region between two nodes is always equal to the distance between the nodes. For the algorithms used in this study, the width of the transport region is equal to the width of the node volume, and all node volumes are defined such that all adjacent nodes have the same widths for each direction. For Figure 3.1, the thermal gradient between the two node centers can be approximated as

$$\left. \frac{\partial T}{\partial x} \right|_{AB} \cong \frac{T_B - T_A}{\Delta x} \quad (3.2)$$

where Δx is the distance between the two node centers.

For the geometry shown in Figure 3.1, the cross sectional area of heat flow between the two nodes will be

$$A = \Delta y \cdot \Delta z \quad (3.3)$$

where Δy and Δz are the widths of the node volume in the y and z direction respectively.

Equations 3.2 and 3.3 can then be substituted into equation 3.1a to describe heat flow from node **A** to node **B** as a function of node properties.

$$q_x^{AB} = k \cdot \frac{\Delta y \cdot \Delta z}{\Delta x} \cdot (T_A - T_B) \quad (3.4)$$

By defining Z_x^{AB} as the thermal impedance between points **A** and **B** in the x direction as shown below,

$$Z_x^{AB} = \frac{\Delta x}{k \cdot \Delta y \cdot \Delta z} \quad [w / K] \quad (3.5)$$

equation 3.4 can then be represented as

$$q_x^{AB} = \frac{T_A - T_B}{Z_x^{AB}} \quad (3.6)$$

In practice, each node will experience heat conduction through all adjacent nodes. The net heat flow into a node will be the sum of heat flow from these adjacent nodes. Equation 3.7 demonstrates the notation used for this study for defining and accounting for the properties of surrounding nodes.

$$q_i^{net} = \sum_j q_{ij} \quad (3.7)$$

In this notation, **i** refers the center node while **j** refers to each of the surrounding nodes. Equation 3.6 can be represented in this form as shown in equation 3.8.

$$q_i^{net} = \sum_j \frac{T_j - T_i}{Z_{ij}} \quad (3.8)$$

Figure 3.2 shows how these elements can be used in a three dimensional rectangular node array.

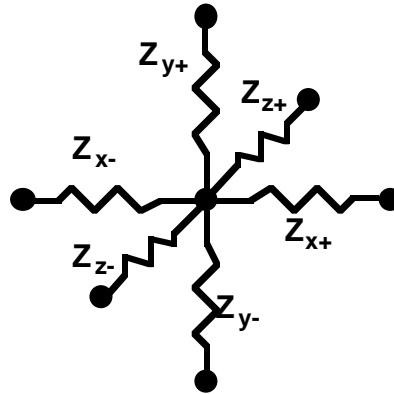


Figure 3.2 Adjacent nodes in a three dimensional rectangular grid.

Under steady state conditions, the net heat flux into the node will be zero ($q^{\text{net}} = 0$) and the node temperature will remain constant with time. In the case where there is no heat generation from within the node, the following relation is true.

$$\sum_j \frac{T_j - T_i}{Z_{ij}} = 0 \quad (3.9)$$

Under steady state conditions in which heat is being generated from within the node, the balance of heat can be represented as equation 3.10

$$q_i + \sum_j \frac{T_j - T_i}{Z_{ij}} = 0 \quad (3.10)$$

where q_i is the heat generation from within the node. By solving for T_i from equation 3.10, equation 3.11 shows that a steady state node temperature can be calculated if the

adjacent node temperatures and the respective thermal impedances between the node centers are known.

$$T_i = \frac{q_i + \sum_j \frac{T_j}{R_{ij}}}{\sum_j \frac{1}{R_{ij}}} \quad (3.11)$$

This equation is used for the Gauss-Seidel iteration [2] technique for computing the temperature profile of a grid of nodes. To use this technique, the region must be divided into regularly shaped node regions in which the thermal impedance between adjacent nodes can be calculated. For this study, all node volumes were rectangular blocks defined within a rectangular coordinate system. Given a set of boundary conditions, this equation can be used to calculate the temperature of each node in sequence. The temperature at each node is then calculated again using the newly computed temperature of the adjacent nodes. This process is repeated until the temperature values do not change from additional iterations.

3.2 Grid Arrangements

Further discussion of the numerical modeling methods used for this study requires an explanation of some of the conventions used in the computer program called "HEAT" that was written for this project. Appendix A explains the details of how to use this program and describes its functions.

Input for the program is given by a configuration file which supplies the following information:

1. Grid arrangement
2. Boundary conditions
3. Material attributes list, which contains the thermal conductivity (k) for each material used. Transient analyses also use heat capacity (C) values
4. Element list, which contains the boundary coordinates for each element and lists what material each block is made of

Table 3.2 Information contained in HEAT configuration file.

For this study, the word **element** refers to a rectangularly shaped region of a single material, and will generally contain many nodes. The "HEAT" program defines the device boundaries as a set of these elements. Each node within an element is assigned material attributes associated with that element. Figure 3.3 and Figure 3.4 show a representation of a bismuth microbolometer with gold leads on a quartz substrate. The bismuth film shown in figure 3.4 is divided into two elements (#1 and #2), where element #1 contains the nodes where power is dissipated, while element #2 is passive. While joule heating does occur everywhere in the electrical circuit, almost all power is dissipated within the heater element. The models presented here assume that all power is distributed uniformly within all the elements designated as heater elements. The HEAT program adds up the total volume of heater elements and divides the total input power by this volume to compute the power density.

Figure 3.4 illustrates how symmetry can simplify the problem by reducing the volume that needs to be modeled. When only one-half or one-fourth of the device is

modeled (due to symmetry), then the total power listed in the configuration file needs to be reduced by one-half or one-fourth, respectively.

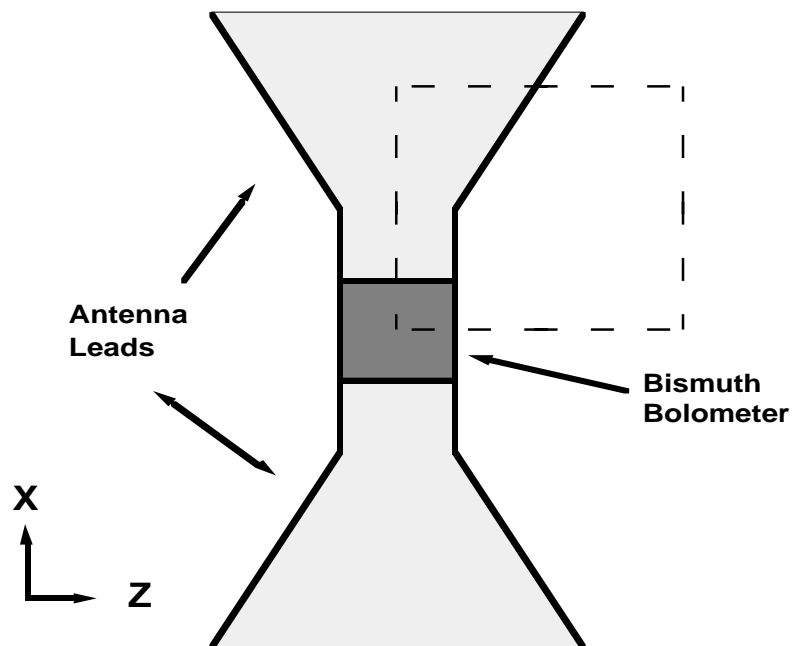


Figure 3.3 Overhead view of an antenna-coupled bismuth microbolometer. For thermal simulations, only the dashed region needs to be modeled, due to symmetry.

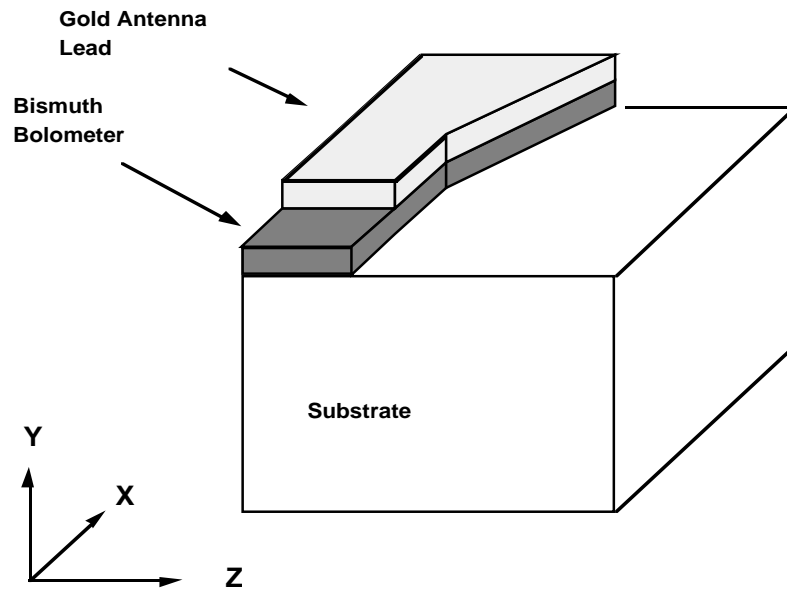


Figure 3.4 Thermally active region for an antenna-coupled bismuth microbolometer

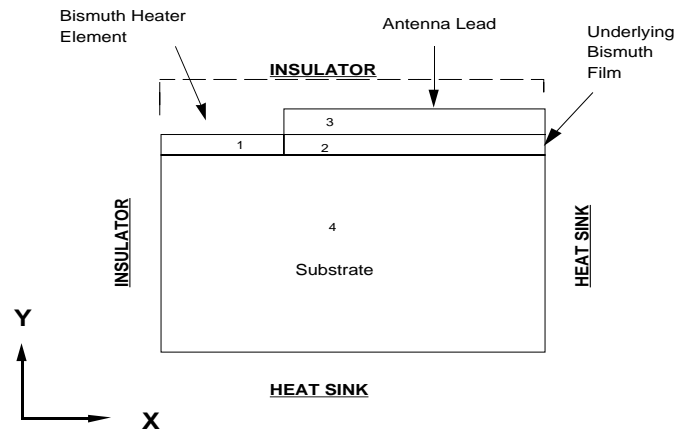


Figure 3.5 Layout of elements used for analyzing a bismuth microbolometer

Temperature profile computation takes place in two phases. In the first phase, the impedance between each adjacent node is calculated and stored in an array. The second phase involves calculating a temperature value for each node using the Gauss-Seidel iteration method described earlier. To compute the node-to-node impedances in a homogeneous region, equation 3.12 is used, where \mathbf{k} is the thermal conductivity of the material in which the node lies, $\Delta\mathbf{L}$ is the distance between the two nodes, and $\Delta\mathbf{i}$ and $\Delta\mathbf{j}$ ($\Delta\mathbf{y}$ and $\Delta\mathbf{z}$ in figure 3.1b) are the lateral dimensions of the transport region between the nodes. The lateral boundaries (width) of the transport region lies at the node volume boundary, and is normally defined as halfway between the lateral nodes.

$$Z = \frac{1}{k} \cdot \frac{\Delta L}{\Delta i \cdot \Delta j} \quad (3.12)$$

In order to allow flexibility in defining device structures, the HEAT program accounts for material boundaries that fall arbitrarily between node centers. Figure 3.6 shows an example where a material boundary lies between two adjacent nodes. In computing the impedance across a boundary, the material on both sides must be accounted for. In this case, the net impedance is just the sum of the two impedances on either side of the boundary.

$$Z = \frac{1}{k_I} \cdot \frac{\Delta L_I}{\Delta i \cdot \Delta j} + \frac{1}{k_{II}} \cdot \frac{\Delta L_{II}}{\Delta i \cdot \Delta j} \quad (3.13)$$

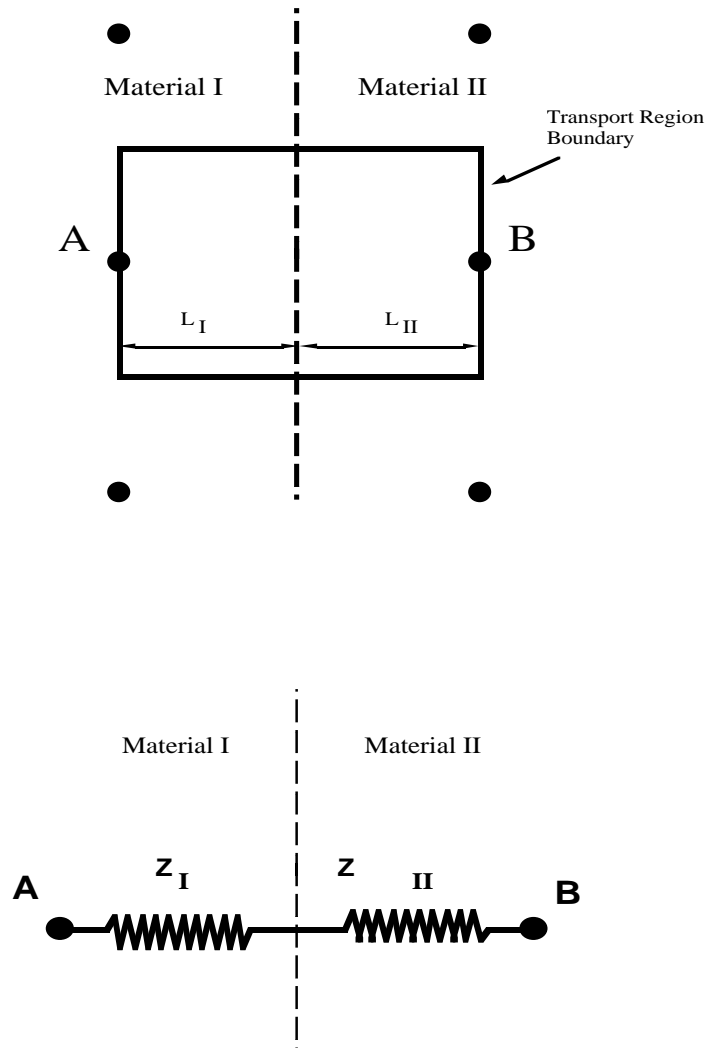


Figure 3.6 Accounting for material boundaries placed between node centers.

As mentioned earlier, the lateral boundaries of the transport region are normally chosen to lie halfway between the center node and the adjacent nodes. An exception to this rule is when the adjacent node center lies within another material. In this case, the node boundary is chosen to lie at the material boundary. Using this rule avoids the possibility of having a node impedance made up of two materials in parallel. An example of an application of this rule is when a material boundary lies parallel to the transport region of two nodes. Since the transport region excludes the material on the other side of the boundary, only one material needs to be considered in this case. This also simplifies the case where multiple orthogonal boundaries fall between a node and its adjacent nodes. For example, along the edge of a device, there can be at least two boundaries between adjacent nodes. By defining the boundary in the lateral direction at the material boundary, the problem of calculating the transverse impedance is reduced to the case of only two materials in series. This rule also applies to the corners of a device where three orthogonal boundaries lie. Again, the problem is reduced to the case of only two materials in series.

In some cases, a material boundary will fall directly on a plane of nodes. In this instance, the node center will be considered to be of the same material as the lateral element that was defined in the HEAT configuration file.

3.3 Transient Analysis

3.3.1 Introduction to Transient Analyses

Since knowing the speed of a detector response is often important for many applications, it is useful have a transient thermal model for predicting microbolometer performance as a function of frequency. Typical methods for time dependent analysis involve time-stepping through the heat flow processing a small interval of time. Each pass will simultaneously increment a time step while iterating the temperature calculation between each node. A smaller time interval will increase the accuracy while increasing the computation time.

The time stepping techniques, though commonly used, can be somewhat awkward when analyzing over a wide range of times. For example, if the same time increment is used for all solutions, then the computation time will increase linearly with the final response time being solved for. A thermal profile at 1 kilohertz will require ten times the computation time for a profile at 10 kilohertz. A longer time interval can sometimes be used to speed the computation time at lower frequencies. However, stability considerations sometimes limit the choice of interval time, so that low frequency analysis can be impractical.

A new algorithm will be presented here that approximates the transient thermal response of a system of nodes without time-stepping. The method does involve repeating iterations over the set of nodes, but will theoretically require the same computation time for a point in time. The method also appears to be inherently stable, and does not have any time constraints. This method, as well as a conventional time-stepping method will be explained later in this chapter. Assumptions and mechanisms are explained, and results of this method for simple geometries are presented and compared to analytical results.

3.3.1 Transient Thermal Mechanisms

The thermal energy exchange between two nodes over a time span of $\Delta\tau$ can be approximated as

$$Q_{AB} = \frac{\Delta T}{Z} \Delta \tau \quad (3.14)$$

where ΔT is the temperature difference between the two nodes. This relation will be accurate as long as ΔT remains nearly constant throughout the time period. For a dynamic system, a small value of $\Delta \tau$ can usually be chosen so that the temperature gradient remains nearly constant for that time period.

Using the nodal notion used in equation 3.8, the net gain in thermal energy due to a temperature difference between a small volume and its surroundings over a time period of Δt , can be represented as

$$Q_i^{\text{net}} = \Delta \tau \cdot \sum_j \frac{T_j - T_i}{Z_{ij}} \quad (3.15)$$

The temperature change that a small volume will experience due to a change in thermal energy can be expressed as

$$\Delta T = \int_0^Q \frac{1}{(\rho \cdot c \cdot V)} dE \quad (3.16a)$$

where

$$Q \equiv \text{Net heat accumulation [watts} \cdot \text{sec]} \quad (3.16b)$$

$$\rho = \text{density [g/cm}^2\text{]} \quad (3.16c)$$

$$c = \text{specific heat [w} \cdot \text{sec / K / g]} \quad (3.16d)$$

$$V = \text{volume of region [cm}^2\text{]} \quad (3.16e)$$

The $\rho c V$ term is also known as the heat capacitance (C).

$$C = \rho \cdot c \cdot V \quad (3.17)$$

For systems in which the $\rho c V$ term is nearly constant throughout the temperature range (this is generally true for small temperature changes), equation 3.16 can be approximated as:

$$\Delta T_i = \frac{Q_i}{C_i} \quad (3.18)$$

by treating the volume as a lumped element.

For steady state analyses, the node temperatures were solved under conditions in which the temperature remained constant with time. Under this criterion, the nodes experience no change in thermal energy over time. For transient analyses, an energy balance for a passive node can be represented as

$$\Delta\tau \cdot \sum_j \frac{T_j^p - T_i^p}{Z_{ij}} = C_i \cdot [T_i^{p+1} - T_i^p] \quad (3.19)$$

where each side represents the net increase in thermal energy during the time interval $\Delta\tau$. The superscripts **p** and **p+1** refer to values immediately before and after the time interval $\Delta\tau$. For an active node which generates heat, the heat balance can be approximated as

$$\Delta\tau \cdot q_i + \Delta\tau \cdot \sum_j \frac{T_j^p - T_i^p}{Z_{ij}} = C_i \cdot [T_i^{p+1} - T_i^p] \quad (3.20)$$

This equation is referred to as the forward-difference [2] or explicit relation since the temperature difference between the nodes is used to predict the future temperature of the node. A backwards-difference (implicit) relation also exists, and is represented as

$$\Delta\tau \cdot q_i + \Delta\tau \cdot \sum_j \frac{T_j^{p+1} - T_i^{p+1}}{Z_{ij}} = C_i \cdot [T_i^{p+1} - T_i^p] \quad (3.21)$$

The solution for T_i^{p+1} in each of these equations is given by equations 3.22 and 3.23 respectively.

$$T_i^{p+1} = \left(q_i + \sum_j \frac{T_j^p}{Z_{ij}} \right) \cdot \frac{\Delta\tau}{C_i} + \left(1 - \frac{\Delta\tau}{C_i} \cdot \sum_j \frac{1}{Z_{ij}} \right) \cdot T_i^p \quad (3.22)$$

$$T_i^{p+1} = \frac{q_i + \sum_j \frac{T_j^{p+1}}{Z_{ij}} + \frac{T_i^p \cdot C_i}{\Delta\tau}}{\sum_j \frac{1}{Z_{ij}} + \frac{C_i}{\Delta\tau}} \quad (3.23)$$

It can be shown that both of these equations will oscillate for sufficiently large values of $\Delta\tau$, and will even become unstable for the explicit expression. For example, for regions where $q_i = 0$, the stability requirement for equation 3.22 becomes

$$\Delta\tau \leq \frac{C_i}{\sum_j \frac{1}{Z_{ij}}} \quad (3.24)$$

Algebraic manipulation will show that choosing a $\Delta\tau$ above this threshold will result in a node temperature that is higher than the steady state solution for that iteration. A similar argument can be made to show oscillating behavior in equation 3.23 for high values of $\Delta\tau$. Equation 3.25 shows the maximum time increment ($\Delta\tau_{\max}$) in terms of material properties and node spacing for a node contained within a three dimensional rectangular network of a homogeneous material for the explicit expression.

$$\Delta\tau_{\max} = \frac{p \cdot c \cdot \Delta s^2}{6 \cdot k} \quad (3.25)$$

The above formula assumes that the center node is surrounded by six adjacent nodes which are equidistant from the center node. The distance between the center node and the adjacent nodes is Δs . Table 3.2 shows tabulated values of $\Delta\tau_{\max}$ for a node spacing of $0.1\mu\text{m}$ for various materials used in fabricating microbolometers.

Material	density ρ (g/cm ³)	specific heat c (w·s/g)	thermal conductivity k (w/cm/K)	$\Delta\tau_{\max}$ (s)
Au	19.3 ¹	0.1292 ¹	3.15 ¹	1.3 x 10 ⁻¹¹
Ag	10.5 ¹	0.234 ¹	4.268 ¹	9.6 x 10 ⁻¹²
Bi	9.80 ²	0.124 ²	0.0792 ²	2.6 x 10 ⁻¹⁰
SiO ₂ (fused silica)	2.203 ¹	0.747 ¹	0.014 ¹	1.5 x 10 ⁻⁹
Al ₂ O ₃ (300K)	3.99 ¹	0.774 ¹	0.110 ¹	4.7 x 10 ⁻¹⁰
Al ₂ O ₃ (85K)	~4	0.293 ⁵	~8 ⁴	2.4 x 10 ⁻¹⁰
GaAs	5.3164 ¹	0.322 ¹	0.586 ¹	4.8 x 10 ⁻¹¹
Te	6.25 ²	0.201 ²	~0.1 ^{2,3}	2.1 x 10 ⁻¹⁰

Table 3.2 Thermal properties of various materials used to make microbolometers and the corresponding maximum stable time increment for a three-dimensional rectangular node matrix with a spacing of 0.1 μm

1 Materials Handbook for Hybrid Microelectronics, Artech House, 1988

2 CRC Handbook of Chemistry and Physics, 64th edition, CRC Press, 1984.

3. Average value of the two values from parallel and perpendicular to the c-axis.

4. Thermophysical Properties of Matter; (volume 2), Thermal Conductivity, Non-metallic Solids, IFI/Plenum, 1970.

5. Thermophysical Properties of Matter; (volume 5), Specific Heat, Non-metallic Solids, IFI/Plenum, 1970.

The table above reveals that the maximum time increment is generally limited by the materials used as the electrical leads (gold and silver). Based on the information above, a kilohertz response at room temperature will require $\sim 10^8$ iterations on a 0.1 μm grid if Au or Ag are considered. If only bismuth is considered, it still would take over 10^6 iterations if a 0.1 μm grid size is used. This table also shows that some substrate materials may limit the time increment when used near liquid nitrogen temperatures. Increasing the grid size would allow longer time increments, but lowers the accuracy, and may not be possible for devices with small structures.

Although the implicit expression is known to be inherently stable, it will exhibit damped oscillations with each iteration for large values of $\Delta\tau$. The intensity of the oscillations and the dampening time constant will increase as $\Delta\tau$ is increased.

3.3.3 New Transient Modeling

The possibility of using an algorithm which does not use the time increment technique was investigated as a means to further study the transient response of microbolometers. The mathematics behind the algorithm that was developed is now presented. Here is a summary of the thought process behind the development of the algorithm that will be presented: The algorithm will assume that the energy exchanged between two nodes can be represented in convenient form. This form can be easily solved except for one unknown function. A trial solution for this unknown function was then found by solving for a special case with specified boundary conditions. This function was then integrated into an algorithm to compute the energy exchange for a macroscopic system of nodes. The algorithm was then used to compute thermal profiles for node systems which could be solved analytically. To test the validity of the algorithm, the numerical results were compared to the analytical solutions.

The energy balance for a node that has experienced a transient thermal effect can be represented with the following equation

$$\mathbf{q}_i \cdot \Delta\tau + \mathbf{Q}_i^{\text{net}} = \mathbf{C}_i \cdot T_i(\tau) \quad (3.26)$$

This equation is valid even for long periods of time. It is assumed that the rate of internal heat generation (\mathbf{q}_i) remains constant, and the heat capacity of the node (\mathbf{C}_i) also remains constant over the time and temperature range. The initial temperature of the node is set at zero. The middle term $\mathbf{Q}_i^{\text{net}}$ refers to the net thermal energy exchange that the node receives from the surrounding nodes, and can be expressed as the sum of the energy transfer from each adjacent node.

$$Q_i^{\text{net}}(\tau) = \sum_j Q_{ij}(\tau) \quad (3.27)$$

where the energy transfer between each node can be represented as

$$Q_{ij}(\tau) = \int_0^{\tau} q_{ij}(t) dt \quad (3.28)$$

The algorithm relies on the assumption that the energy exchange between two nodes after time τ can be represented as

$$Q_{ij}(\tau) = \tau \cdot \frac{T_j(\tau) - T_i(\tau)}{Z_{ij}} \cdot \Gamma_{ij}(\tau) \quad (3.29)$$

where Γ_{ij} is a function which relates the net heat exchange between two nodes to the final temperature difference. This solution to the function is known, and must be solved.

All solutions to time dependent thermal systems must satisfy the following governing equation.

$$\frac{dT}{dt} = \alpha \cdot \nabla^2 T \quad (3.30)$$

The α term is also known as the thermal diffusivity, and can be related to other physical properties as

$$\alpha = \frac{k}{\rho \cdot c} \quad (3.31)$$

In order to find a solution for Γ_{ij} , a trial solution is found by solving for a special case of specified boundary conditions. Temperature profiles calculated from this solution are computed for more general cases and compared to analytical results.

Consider the case of constant heat flux into a semi-infinite slab of homogeneous material. By using a Laplace transform technique [3], the temperature profile can be shown to be

$$T(x,t) = \frac{2 \cdot q_o}{k \cdot A} \cdot \sqrt{\frac{\alpha \cdot t}{\pi}} \cdot \exp\left(\frac{-x^2}{4 \cdot \alpha \cdot t}\right) - \frac{q_o \cdot x}{A \cdot k} \cdot \operatorname{erfc}\left(\frac{x}{2 \cdot \sqrt{\alpha \cdot t}}\right) \quad (3.32)$$

where $T(x,t)$ is the temperature above ambient, A is the area of the surface, and q_o is the flux at the surface. It is sometimes helpful to represent some relations in terms of diffusion lengths (L_D), defined as

$$L_D = (\alpha \cdot t)^{1/2} \quad (3.33)$$

Equation 3.32 can now be represented as

$$T(x, L_D) = \frac{2 \cdot q_o \cdot L_D}{k \cdot A \cdot \pi^{1/2}} \cdot \exp\left(\frac{-x^2}{4 \cdot L_D^2}\right) - \frac{q_o \cdot x}{A \cdot k} \cdot \operatorname{erfc}\left(\frac{x}{2 \cdot L_D}\right) \quad (3.34)$$

Figure 3.7 shows the temperature profile for this case. Appendix B shows the formula used to compute the complimentary error function (erfc) for the HEAT program, as well as for this graph.

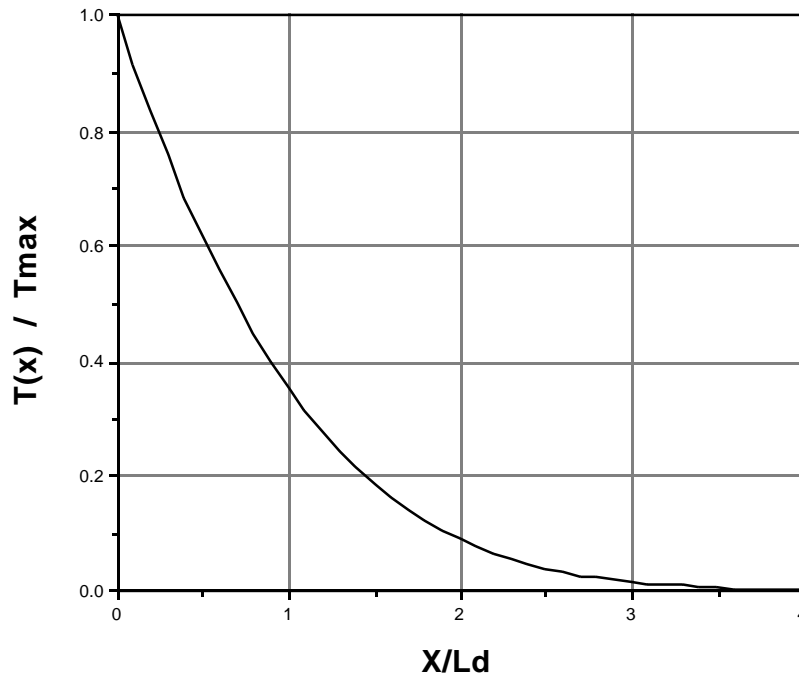


Figure 3.7 Temperature profile into a semi-infinite solid which experiences a constant heat flux at the surface

By using Fourier's law (equation 3.1), the heat flux as a function of x can be determined by taking the derivative of the temperature (equation 3.32 or 3.34) with respect to x . By using the following identities

$$\frac{d}{dB}(\operatorname{erfc}(B)) = -\frac{d}{dB}(\operatorname{erf}(B)) \cdot dB \quad (3.35)$$

$$* \quad \frac{d}{dB}(\operatorname{erf}(B)) = \frac{2}{\pi^{1/2}} \cdot \exp(-B^2) \cdot dB \quad (3.36)$$

* Ozisik, M Necati, *Heat Conduction*, , New York, John Wiles and Sons, Inc., 1993, page 205

the heat flux can be shown to be

$$q(x, L_D) = q_o \cdot \operatorname{erfc}\left(\frac{x}{L_D}\right) \quad (3.37)$$

$$q(x, t) = q_o \cdot \operatorname{erfc}\left(\frac{x}{2 \cdot \alpha^{1/2} \cdot t^{1/2}}\right) \quad (3.38)$$

The total energy exchange through a plane that is distance x from the surface will be

$$Q(x, \tau) = \int_0^\tau q_o \cdot \operatorname{erfc}\left(\frac{x}{2 \cdot \alpha^{1/2} \cdot t^{1/2}}\right) dt \quad (3.39)$$

The solution to this problem is detailed in Appendix C, and is as follows

$$Q(x, \tau) = q_o \cdot \left\{ \left(\tau + \frac{x^2}{2 \cdot \alpha} \right) \cdot \operatorname{erfc}\left(\frac{x}{2 \cdot \alpha^{1/2} \cdot \tau^{1/2}}\right) - \frac{x \cdot \tau^{1/2}}{\alpha^{1/2} \cdot \pi^{1/2}} \cdot \exp\left(\frac{-x^2}{4 \cdot \alpha \cdot \tau}\right) \right\} \quad (3.40)$$

Now, let's take a look at how these formulas relate to heat transfer between nodes on a grid. Figure 3.8 plots the location and temperature of three points of reference within a semi-infinite slab. Note that the amount of heat transferred from point **B** to point **A** will be the same as the energy transferred from point **C** to point **A**.

$$Q_{CA}(\tau) = Q_{BA}(\tau) \quad (3.41)$$

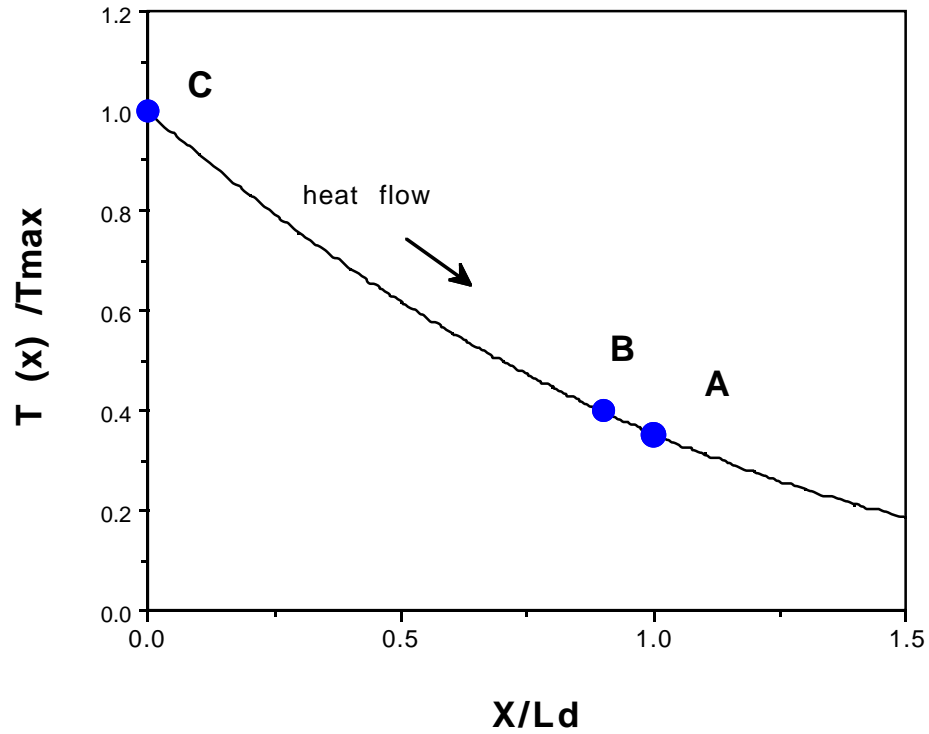


Figure 3.8 Heat transfer between nodes on a grid

By using the solution in equation 3.40 as the left side of equation 3.29, Γ_{ij} can be solved for this case as

$$\Gamma_{ij}(\tau) = \frac{q_o \cdot \left(\tau + \frac{s^2}{2 \cdot \alpha} \right) \cdot \operatorname{erfc} \left(\frac{s}{2 \cdot \alpha^{1/2} \cdot \tau^{1/2}} \right) - \frac{s \cdot \tau^{1/2}}{\pi^{1/2}} \cdot \exp \left(\frac{-s^2}{4 \cdot \alpha \cdot \tau} \right)}{\tau \cdot \frac{\Delta T}{Z_{ij}}} \quad (3.42)$$

where s refers to the distance from the surface of constant flux

For points **A** and **B** in figure 3.8

$$q_{BA}(\tau) \approx \frac{T_B(\tau) - T_A(\tau)}{Z_{BA}} \quad (3.43)$$

For the case shown, q_{BA} was solved as equation 3.38. By substituting equation 3.38 as the $\frac{\Delta T}{Z_{ij}}$ term, Γ_{ij} now can be expressed as

$$\Gamma_{ij}(B) = \frac{(1 + 2 \cdot B^2) \cdot \text{erfc}(B) - \frac{2}{\pi^{1/2}} \cdot B^{1/2} \cdot \exp(-B^2)}{\text{erfc}(B)} \quad (3.44)$$

where

$$B = \frac{s^{1/2}}{2 \cdot \alpha^{1/2} \cdot \tau^{1/2}} \quad (3.45)$$

Figure 3.9 shows a graph of this function compared to the complementary error function.

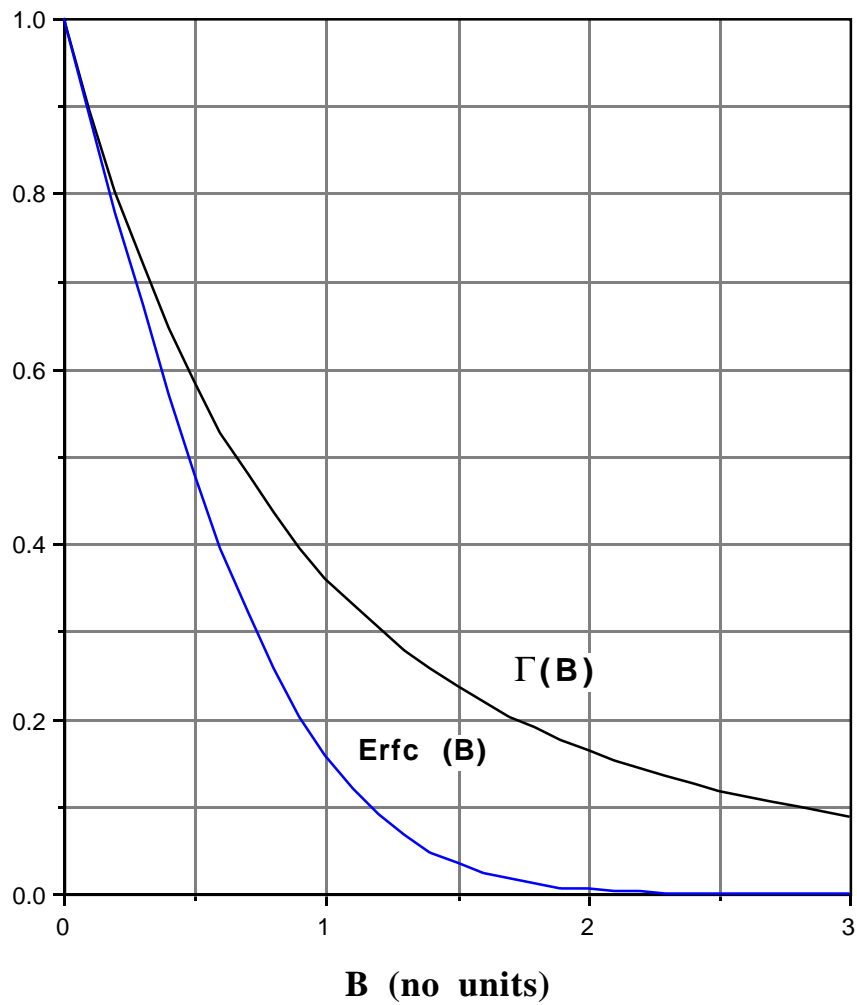


Figure 3.9 Plot of the solution to Γ (as defined by equation 3.44) and the complimentary error function (**erfc**)

3.3.4 Algorithm

To use this model in an algorithm, the thermal impedance (Z_{ij}) and gamma function (Γ_{ij}) is computed for each adjacent node combination.

The energy balance becomes

$$\tau \cdot q_i + \tau \cdot \sum_j (T_j(\tau) - T_i(\tau)) \cdot \frac{\Gamma_{ij}(\tau)}{Z_{ij}} = C_i \cdot T_i(\tau) \quad (3.46)$$

Based upon the assumptions that were made, there are two criteria which must be met in order for the solution of Γ_{ij} (shown in equation 3.44) to be accurate. First, the heat flux at the node must be accurately described by equation 3.43. This can be met for all nodes by requiring that each node be spaced reasonably close to each other. Reasonably close can mean somewhere less than a diffusion length apart. The second criteria is that the heat source, that was designated as being distance s from the node, must remain nearly constant.

The node to node impedances can be divided by the corresponding Γ_{ij} to obtain an effective impedance which will be used for each computation.

$$Z_{ij}^{eff} = \frac{Z_{ij}}{\Gamma_{ij}} \quad (3.47)$$

This Z_{ij}^{eff} remains unchanged throughout the iterations.

Solving for $T_i(\tau)$ gives

$$T_i(\tau) = \frac{q_i + \sum_j \frac{(T_j(\tau) - T_i(\tau))}{Z_{ij}^{eff}}}{\sum_j \frac{1}{Z_{ij}^{eff}} + \frac{C_i}{\tau}} \quad (3.48)$$

Note that the steady state limit ($\tau \rightarrow \infty$, $\Gamma \rightarrow 1$) for this equation becomes identical to the steady state relation shown in equation 3.11.

When computing the value of Γ_{ij} , equation 3.44 requires a single value for diffusivity (α) between every set of adjacent nodes. Although this value is a material property and is independent of the node transport region geometry, this does require some consideration for material boundaries which fall between nodes. For this case, the HEAT program linearly interpolates values of diffusivity in a similar manner as it does with the node to node impedances.

3.3.5 Analysis

The algorithm presented here uses this solution to describe the energy exchange between all nodes by assuming that the rate of heat exchange remains nearly constant throughout the time period. The accuracy of this assumption can be quantified in examining the case of constant heat flux into a semi-infinite solid. A figure of merit (F) can be assigned by dividing the average heat flux by the heat flux at time = τ .

$$F = \frac{q_{ave}(x, \tau)}{q(x, \tau)} \quad (3.49)$$

A value of near one would suggest good agreement with this approximation. For the case of constant heat flux into a semi-infinite solid, the heat flux at τ within the solid is given in equation 3.38, while the average heat flux can be calculated as

$$q_{ij}^{ave}(\tau) = \frac{Q_{ij}(\tau)}{\tau} \quad (3.50)$$

Using these definitions shows that this figure of merit is the same as Γ . The graph of $\Gamma(\mathbf{B})$ (figure 3.9) suggests that this approximation may be adequate for values of \mathbf{B} less than 0.5, or

$$s < (\alpha \cdot \tau)^{1/2} \quad (3.51)$$

$$s < L_D \quad (3.52)$$

where s is the distance from the surface of constant flux. This suggests that the model will be accurate near the sources of heat generation (where temperatures are highest) and less accurate with increasing distance from the heat sources. From an engineering viewpoint, this type of solution may suffice if only the warm regions are of interest.

Figure 3.10 shows temperature profiles computed using this algorithm overlaid with the analytical solution for a constant heat flux into a semi-infinite solid. The analytical profile was computed using equation 3.32. The heat program approximated a semi-infinite slab as a thick ($\gg L_D$) slab of finite thickness with a heat sink at the end. The heat source modeled was a stepped pulse of constant flux at the surface. The time values quoted in the graphs refer to the length of the pulse. The graphs show temperature profiles at the end of the pulse. The solid line represents the analytical solution, while the boxes represent values computed using the algorithm in equation 3.48.

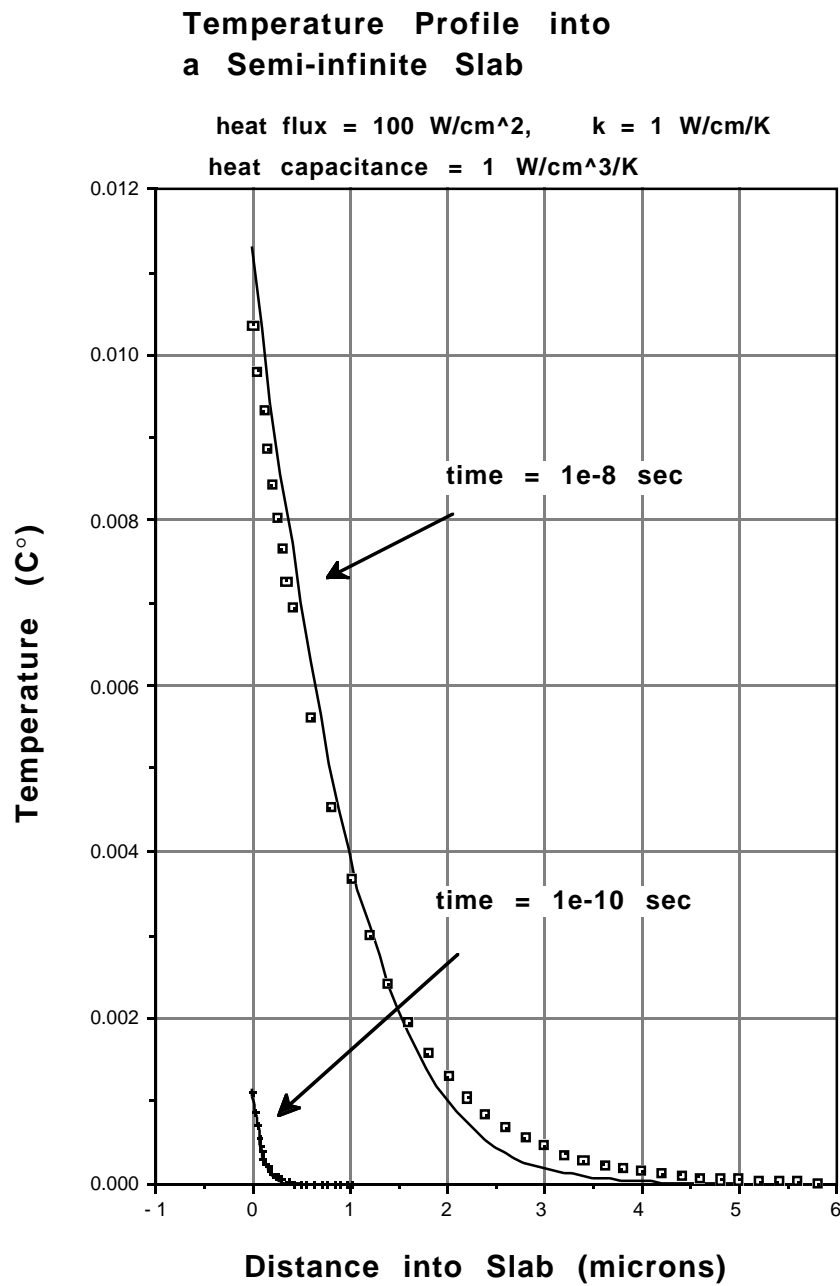


Figure 3.10 Temperature profile into a semi-infinite solid with constant heat flux into the surface. The solid line represents the analytical solution, while the boxes represent values computed using the algorithm in equation 3.48.

Table 3.3 shows parameters that quantify comparisons of the results from this model to the analytical solution. The values of Q_{model} were calculated by integrating the curve.

time (s)	Analytical T_{max} (K)	Model T_{max} (K)	$\frac{T_{\text{model}}}{T_{\text{analytical}}}$	Analytical Q [J]	Model Q [J]	$\frac{Q_{\text{model}}}{Q_{\text{analytical}}}$
10^{-8}	1.13×10^{-2}	1.01×10^{-2}	0.89	1.0×10^{-14}	9.95×10^{-15}	0.995
10^{-10}	1.13×10^{-3}	9.44×10^{-4}	0.86	1.0×10^{-16}	8.99×10^{-17}	0.899

Table 3.3 Comparisons of results from the transient numerical algorithm compared to analytical results for a constant heat flux into a semi-infinite solid.

Figure 3.11 shows the model's temperature profiles for a finite slab which experiences constant flux at one end, and zero flux at the other end. Table 3.4 gives a quantitative analytical comparison for this configuration. Again, the heat source was a time step function.

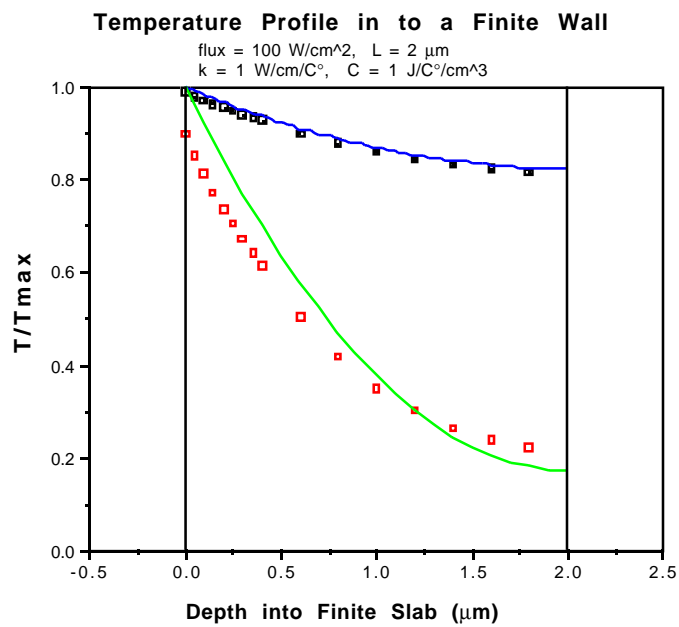
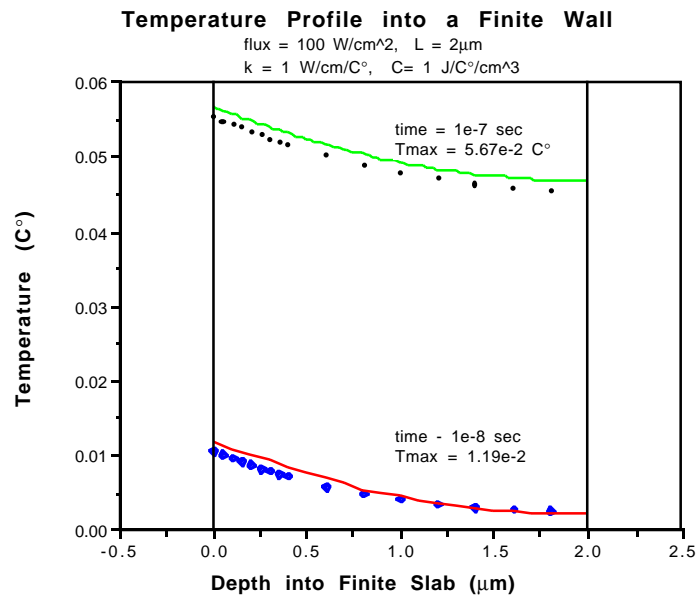


Figure 3.11 Temperature profiles into a finite wall. One wall experiences constant heat flux for $t > 0$, while the other wall is insulated. The solid lines show the analytical solution, while the points show values computed by the algorithm shown as equation 3.32.

time (s)	Analytical T_{\max} (K)	Model T_{\max} (K)	$\frac{T_{\text{model}}}{T_{\text{analytical}}}$	Analytical Q [J]	Model Q [J]	$\frac{Q_{\text{model}}}{Q_{\text{analytical}}}$
10^{-7}	5.57×10^{-2}	5.55×10^{-2}	0.996	1.0×10^{-13}	3.36×10^{-13}	0.836
10^{-8}	1.19×10^{-3}	1.04×10^{-2}	0.87	1.0×10^{-14}	9.71×10^{-14}	0.971

Table 3.4 Comparisons of results from the transient numerical algorithm compared to analytical results for a constant heat flux into a infinite slab.

The analytical solution for this system is found by applying Duhamel's theorem. The solution to this problem is given by Carslaw and Yeager, page 112 [4].

$$T = \frac{q_o \cdot t}{p \cdot c \cdot L} + \frac{q_o \cdot L}{k} \cdot \left[\frac{3 \cdot x^2 - L^2}{k} - \frac{2}{\pi^2} \cdot \sum_{n=1}^{\infty} \left(\frac{(-1)^n}{n^2} \cdot \exp\left(\frac{-\alpha \cdot n^2 \cdot \pi^2 \cdot t}{L^2}\right) \cdot \cos\left(\frac{n \cdot \pi \cdot x}{L}\right) \right) \right] \quad (3.53)$$

For equation 3.53, constant heat flux is introduced into the solid at $x=L$, while no heat flow occurs at $x=0$.

Based on these preliminary tests, it would seem that the model introduced here provides a satisfactory method of computing transient thermal profiles in the vicinity of heat sources without using a time-stepping algorithm. The model and algorithm appear to be a useful technique in predicting transient microbolometer performance.

References

1. S. M. Wentworth, "Far-Infrared Microbolometer Detectors", Doctoral Dissertation, University of Texas at Austin, 1990
2. J. P. Holman, *Heat Transfer*. New York: McGraw-Hill Book Company, 1986.
3. M. N. Ozisik, *Heat Conduction*. New York: John Wiles and Sons, Inc., 1993.
4. H. S. Carslaw, and J. C. Jaeger, *Conduction of Heat in Solids*. Oxford: Clarendon Press, 1959.